JM PAPERS

Two-dimensional response of a floating ice plate to a line load moving at variable speed

Roger J. Hosking[1] and Fausto Milinazzo[2],†

[1]School of Mathematical Sciences, University of Adelaide, Adelaide SA 5005, Australia
[2]Department of Mathematics, Royal Roads Military College, FMO Victoria, BC V0S 1B0, Canada

We significantly extend the results of Miles & Sneyd (*J. Fluid Mech.*, vol. 497, 2003, pp. 435–439) for an accelerating line load on a floating ice plate in their simple linear mathematical model by proceeding to numerical calculations for the response due to a decelerating load. Our results show: (i) how the deflections produced by an impulsively started steadily moving line load begin to develop and eventually approach the well-known steady load-speed-dependent quasi-static and wave-like forms, including above the shallow water gravity wave speed where the shadow zone evolves; (ii) the singularity in the deflection predicted in the simple linear model when the load moves steadily is indeed avoided by a uniformly accelerating load, where the magnitude of the deflection continually increases and its maximum lags a little further behind as the load moves through the critical speed and beyond; (iii) there is also no singularity in the deflection due to a uniformly decelerating load, but whereas the response from a subcritical starting speed is preserved and travels with the load, the magnitude of the deflection may become quite large near a load starting from supercritical speed and approaching rest, which is attributed to constructive interference (reinforcement) as erstwhile trailing, predominantly gravity, waves catch up with the load. While this reinforcement poses no risk to Hercules transport aircraft landing on the thick sea ice at McMurdo Sound, it can account for the reported rapid sinking of the detached cockpit shortly after it came to rest in the 1974 Lockheed Electra aircraft crash in the Canadian Arctic.

Key words: elastic waves, surface gravity waves

1. Introduction

Floating ice covers have been important for transport and field operations in cold regions for many years. For example, in Canada ice roads are used by quite heavy vehicles in winter, and essential supplies for scientists in Antarctica have been delivered by large

† Email address for correspondence: fmilinaz@trilan.ca

Hercules aircraft landing on the ice at McMurdo Sound. Such operations are usually safe, but there have been occasions where vehicles have gone through the ice cover. There is a critical speed for a moving load on an ice cover, associated with a resonant response that can become so large it must be avoided in such operations. On the other hand, the resonance may be exploited to break up an ice cover, as on the Saint Lawrence Seaway using hovercraft. The monograph 'Moving Loads on Ice Plates' by Squire *et al.* (1996) summarised the theory and various field experiments that had been undertaken until 1996, providing scientists and practitioners with a concise source of information and understanding of the ice response, so often very different from that due to a stationary load.

The typical mathematical model in the literature envisages a thin elastic plate floating on an incompressible fluid of finite depth, representing the ice sheet and underlying water, respectively. Predictions from associated linear theory have proven remarkably consistent with field observations by Takizawa and others, including the hierarchy of load speed dependent responses (cf. chapters 5 and 6 of Squire *et al.* 1996) – and there has been recent reconfirmation of the planar wave patterns via remote sensing (cf. Babaei *et al.* 2016; van der Sanden & Short 2017). The critical speed is the minimum phase speed c_{min} of flexural-gravity waves in the system where the resonant response develops over time due to the continual accumulation of energy when the load moves steadily at that speed, since c_{min} coincides with the group speed c_g at the corresponding critical wavenumber k_{min}.

The linear theory for a line load defined the two-dimensional response in the line of motion of the load, but the additional dimension inherent in the theory for a point or distributed load had notable consequences (cf. Nugroho *et al.* 1999). Most notably, the three-dimensional theory showed that the gravity wave speed $\sqrt{gH}$ (where g is the gravitational acceleration and H denotes the water depth) approached as the wavenumber $k \to 0$ is not critical in the sense of c_{min}, and the time evolution of the responses due to an impulsively started load was found to be shorter in general. However, both the two-dimensional and three-dimensional linear theory identified $\sqrt{gH}$ as the lower bound on the load speed for the onset of the so-called shadow zone (cf. Squire *et al.* 1996), where there are no gravity-dominated waves behind the moving load. Drawing a correspondingly higher horizontal line representing a higher load speed V in figure 1 immediately suggests that phenomenon in the two-dimensional line load theory. The quasi-static response universally predicted by the linear theory at subcritical speeds $V < c_{min}$ likewise corresponds to no intersection at all with the phase speed curve by a correspondingly lower horizontal line. (Incidentally, the phase speed and group speed curves are lowered by in-plane stress, which is associated with wave blocking – cf. Das, Sahoo & Meylan (2018).) The inclusion of anelasticity rendered the deflection pronounced but finite at the critical speed and further reduced the evolution time for the respective responses due to an impulsively started steadily moving load, while also accounting for some observed features such as the lag in the maximum depression behind the load and why the planar wave patterns may appear swept back (cf. Squire *et al.* 1996; Wang, Hosking & Milinazzo 2004).

The classical linear theory has mainly addressed the response of a floating ice plate to a steadily moving load or to an impulsively started steadily moving load. An exception is the contribution by Miles & Sneyd (2003), which provides the analysis for the response due to a line load moving with variable speed more thoroughly explored in this article. We initially also adopt Takizawa data in §§ 3 and 4 to re-examine and extend their calculations for impulsively started and uniformly accelerating line loads. Nonlinear theory is not pursued here, but it is notable that numerical results for the evolution of solitary waves
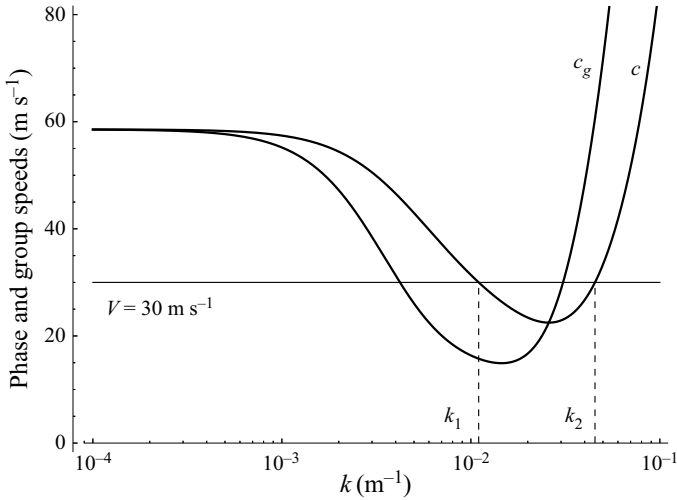
Figure 1. The two branches of the phase speed and group speed curves $c(k)$ and $c_g(k)$ (which are symmetric about the origin $k = 0$) are shown for McMurdo Sound parameters. The values k_1 and k_2 where $c = V$ are the respective wavenumbers of the trailing predominantly gravity and leading predominantly flexural components in the wave pattern previously discussed for loads moving at constant supercritical speeds $V > c_{min}$, where c_{min} denotes the minimum phase speed (cf. Squire *et al.* 1996). For a steadily moving load, the large response at the critical speed corresponds to a continual accumulation of energy at the load, since c_{min} coincides with the group speed c_g at the corresponding critical wavenumber k_{min}. The gravity wave speed $\sqrt{gH}$ in the limit $k \to 0$ defines the threshold for a shadow zone where no gravity-dominated waves arise behind the load (i.e. when $V > \sqrt{gH}$), and the response is quasi-static at subcritical speeds $V < c_{min}$ (cf. Squire *et al.* 1996).

due to a load moving over a finite time appear to show similar responses initially (cf. Guyenne & Parau 2014). However, in this article we also proceed to investigate the recent prediction by Dinvay, Kalisch & Parau (2019) that a load decelerating from supercritical speed may trigger a remarkably large deflection as some quite early field observations suggested in Beltaos (1981), attributed to constructive interference as erstwhile trailing gravity-dominated waves catch up with the slowing load. Landing aircraft typically require approach speeds that exceed the critical speed on ice runways, and land-based vehicles may also drive at supercritical speeds on ice roads (cf. Babaei *et al.* 2016; van der Sanden & Short 2017). The unsteady motion of an air-cushion vehicle and the hard landing of an aircraft on ice covers have previously been considered to some extent in Pogorelova (2008) and Matiushina, Pogorelova & Kozin (2016). Here, we choose to investigate the catchup phenomenon in the context of simulations for the landing of Hercules transport aircraft at McMurdo Sound in the Antarctic and a Lockheed Electra aircraft accident that occurred in the Canadian Arctic.

Reference again to figure 1 provides a premonition of our detailed results, when the horizontal line shown is envisaged to move vertically for a variable load speed, sweeping upward for an accelerating load or downward for a decelerating load. An increasing load speed $V(t)$ (where t denotes the time) above c_{min} may be expected to develop trailing predominantly gravity and leading predominantly flexural waves, supplementing a quasi-static form if the load speed had previously been subcritical ($V < c_{min}$), until the trailing waves are no longer generated when $V > \sqrt{gH}$. Similarly, only the leading waves may be expected when a decreasing load speed exceeds the gravity wave speed $\sqrt{gH}$, but the more complete flexural-gravity wave contribution would then arise if the load enters the supercritical regime $c_{min} < V < \sqrt{gH}$, followed by quasi-static contributions

938 A2-3

if it enters the subcritical regime $V < c_{min}$. Transients produced during a variable load speed phase may be expected to persist for some time, whether or not the load initially or subsequently moves steadily.

2. Deflection due to a line load

As previously discussed, the simple linear two-dimensional model of Miles & Sneyd (2003) is further explored in this article. Thus the equations for the velocity potential $\phi(x, y, t)$ in the underlying water of density ρ and depth H and the deflection $\eta(x, t)$ of the floating thin elastic plate are

$$\frac{\partial^2 \phi}{\partial x^2} + \frac{\partial^2 \phi}{\partial y^2} = 0 \quad (-\infty < x < \infty, -H < y < 0), \tag{2.1}$$

$$D\frac{\partial^4 \eta}{\partial x^4} + \rho g \eta = -\rho \frac{\partial \phi}{\partial t}\bigg|_{y=0} - p(x, t), \tag{2.2}$$

subject to

$$\frac{\partial \phi}{\partial y}\bigg|_{y=-H} = 0, \quad \frac{\partial \phi}{\partial y}\bigg|_{y=0} = \frac{\partial \eta}{\partial t}, \tag{2.3a,b}$$

where D is the flexural rigidity of the plate and $p(x, t)$ is the pressure exerted by the load. The plate acceleration term is ignored (cf. Squire *et al.* 1996). For a line load located at $x = X(t)$ such that $p(x, t) = p_0 \delta(x - X(t))$, the one-dimensional form for the deflection obtained via Fourier–Laplace transforms may be rewritten as – cf. equation (2.13) in Miles & Sneyd (2003)

$$\eta(x, t) = -\frac{p_0}{2\pi\rho} \int_{-\infty}^{\infty} e^{ikx} \frac{\tanh(kH)}{c(k)} \left(\int_0^t \exp(-ikX(\tau)) \sin[kc(k)(t - \tau)] \, d\tau \right) dk, \tag{2.4}$$

where the appropriate positive branch of the phase speed

$$c(k) = \sqrt{\left(\frac{g}{k} + \frac{Dk^3}{\rho}\right) \tanh(kH)} \tag{2.5}$$

is symmetric in the wavenumber k. The time integral in (2.4) may be expressed as

$$\frac{1}{2i} \int_0^t \exp(-ikX(\tau)) \left(\exp(ikc(t - \tau)) - \exp(-ikc(t - \tau))\right) d\tau = \frac{1}{2i} \left[I(c)\exp(ikct)\right.$$
$$\left. -I(-c)\exp(-ikct)\right], \tag{2.6}$$

where

$$I(c) = \int_0^t \exp(-ik[c\tau + X(\tau)]) \, d\tau. \tag{2.7}$$

Thus adopting the real part of interest we have

$$\eta(x, t) = -\frac{p_0}{2\pi\rho} \int_0^{\infty} \frac{\tanh(kH)}{c(k)} \text{Im}\left[I(c)\exp(ik(x + ct)) - I(-c)\exp(ik(x - ct))\right] dk, \tag{2.8}$$

involving the leftward propagating component

$$\eta_-(x, t) = -\frac{p_0}{2\pi\rho} \int_0^{\infty} \frac{\tanh(kH)}{c(k)} \text{Im}\left[I(c)\exp(ik(x + ct))\right] dk \tag{2.9}$$

and the rightward propagating component (in the direction of the load motion)

$$\eta_+(x, t) = \frac{p_0}{2\pi\rho} \int_0^\infty \frac{\tanh(kH)}{c(k)} \text{Im}\left[I(-c)\exp(ik(x - ct))\right] \, dk. \qquad (2.10)$$

3. Impulsively started steadily moving loads

In this section, we consider the evolution of responses to steadily moving line loads that are impulsively started, when implicitly no account is taken of prior loading (cf. Squire *et al.* 1996; Miles & Sneyd 2003). Thus the deflection $\eta(x, t)$ is calculated for loads that are switched on impulsively at time $t = 0$ and then move steadily, such that $X(t) = Vt$, $t > 0$ where V is constant. We adopt Takizawa data similar to Miles & Sneyd (2003) – viz. Young's modulus $E = 1.79 \times 10^8$ Pa, plate thickness $h = 0.14$ m, Poisson ratio $\nu = 1/3$, water density $\rho = 1026$ kg m^{-3} and water depth $H = 6.80$ m. The critical speed c_{min} is a little over 5 m s^{-1}, and the gravity wave speed is $\sqrt{gH} = 8.16$ m s^{-1}. The deflections illustrated in this section are in the frame of motion of the load.

All of the results reported in this article were obtained by analytically evaluating the integral in t that appears in (2.4), and then approximating the inverse Fourier transform by a discrete inverse Fourier transform that produces a set of linear equations relating the deflection at a discrete set of spatial values to the Fourier transform of the deflection at a discrete set of wavenumber values. The fast Fourier transform was employed to solve this system of equations to obtain the deflection. In the case of impulsively started loads, the application of the discrete inverse Fourier transform is justified since the integrand in (2.4) has no poles on the real axis. When the initial condition corresponding to a steadily moving load is introduced, the modified integrand corresponding to (2.4) has poles on the real axis for values of k where $V^2 - c^2 = 0$. The part of the integrand corresponding to the initial conditions must then be modified, so that the contribution from the poles can be calculated analytically and the discrete inverse Fourier transform can be applied to approximate what remains. Appendix A provides further details.

We first present mesh plots that show the evolution of the deflection in the (x, t)-plane, which directly compare figures in Miles & Sneyd (2003) for two illustrative load speeds. The x-axis in metres is again placed in the immediate foreground in figures 2 and 3, but on the second horizontal axis we prefer to represent the equivalent time span in seconds. For an impulsively started load that then moves at the subcritical speed $V = 2$ m s^{-1}, we found the deflection starts to reflect the familiar quasi-static form due to the corresponding steadily moving load, as shown in figure 2, which resembles figure 1(*a*) of Miles & Sneyd (2003). The deflection we obtained for an impulsively started load that then moves at constant supercritical speed $V = 1.17c_{min}$ shown in figure 3 also resembles figure 1(*b*) of Miles & Sneyd (2003), where characteristic leading predominantly flexural waves and trailing predominantly gravity waves appear. The longer time taken for the trailing waves to more clearly emerge is shown in figure 4. The response for a higher impulsively started constant supercritical speed $V = 10$ m s$^{-1} > \sqrt{gH}$ at $t = 8$ s in figure 5 shows that the leading predominantly flexural wave is then accompanied by a trailing transient, which dissipates as the shadow zone emerges, as seen in figure 6. While each of the three different steady-state forms quickly emerge near the load, the emergence of the steady-state takes longer elsewhere – but we recognise the restricted propagation to the line of motion in the two-dimensional model is an extenuating factor. (The present context is accordingly called one-dimensional in Wang *et al.* (2004), where 'one-dimensional' and 'two-dimensional' refer to the flexural-gravity wave propagation in the floating ice plate, but in this paper
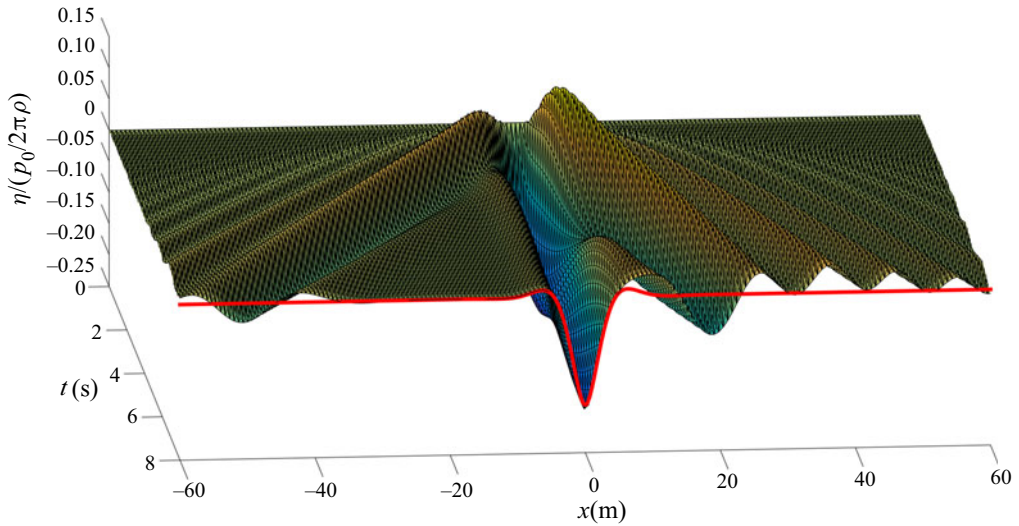
Figure 2. The evolution of the deflection due to an impulsively started steadily moving load at the subcritical speed $V = 2\,\text{m s}^{-1}$ over the first 8 s for the Takizawa data, in a direct comparison with figure 1(a) of Miles & Sneyd (2003). The familiar constant load speed quasi-static form shown in red begins to emerge as the transients propagate away.
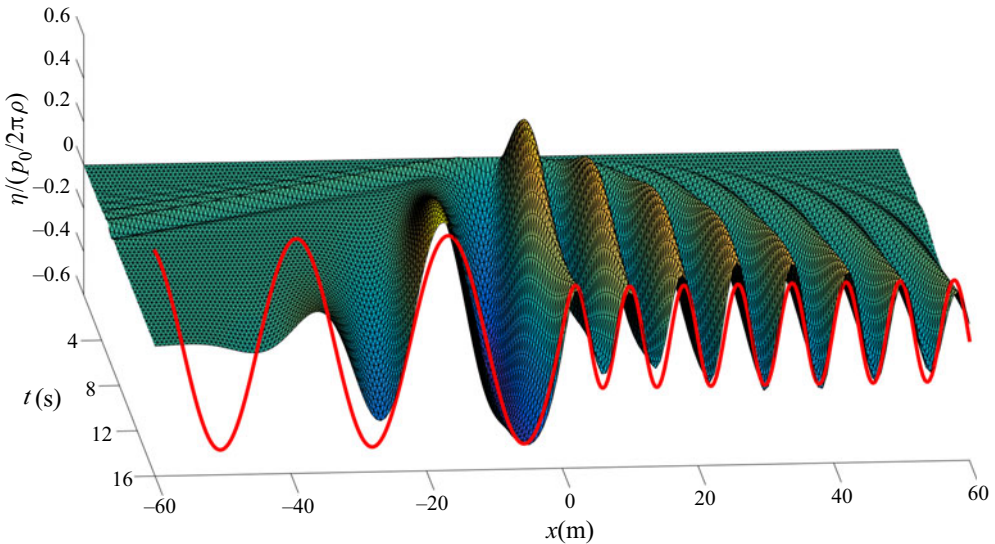

Figure 3. The evolution of the deflection due to an impulsively started steadily moving load at the supercritical speed $V = 1.17c_{min}\,\text{m s}^{-1}$ over the first 16 s for the Takizawa data, in a direct comparison with figure 1(b) of Miles & Sneyd (2003). The familiar constant load speed wave form shown in red begins to emerge as the transients propagate away.

we have used the now more common terminology acknowledging the additional vertical dimension.)

Incidentally, to render the deflections in metres at any time t, the magnitudes shown in our graphical results throughout this paper must be multiplied by the factor $p_0/(2\pi\rho)$ to scale in the load – e.g. the skidoo and driver in Takizawa's experiments on Lake Saroma

938 A2-6

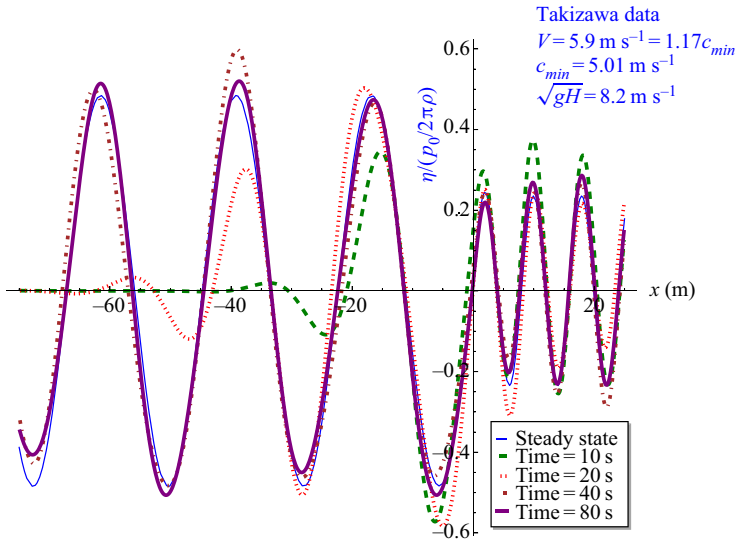Figure 4. The evolution of the deflection at the impulsively started supercritical load speed $V = 1.17c_{min}$ m s^{-1} for the Takizawa data, showing the time taken for the longer trailing predominantly gravity wave to more clearly develop.
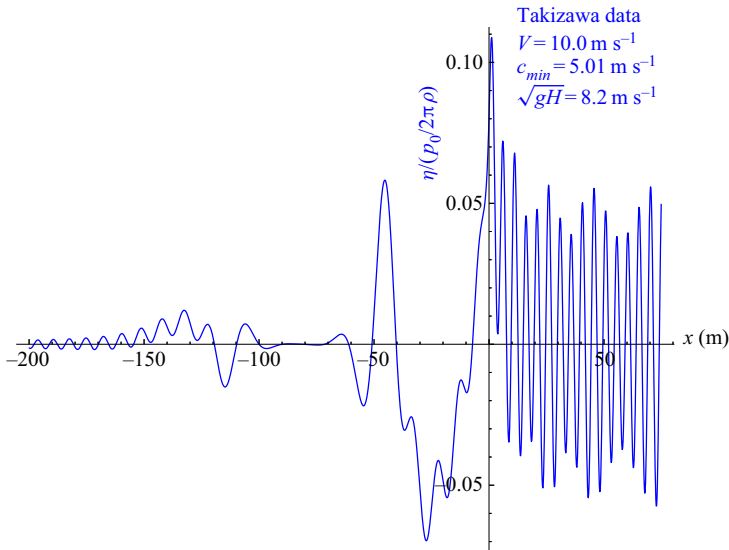

Figure 5. The deflection for the impulsively started higher supercritical load speed $V = 10$ m s$^{-1} > \sqrt{gH}$ at 8 s for the Takizawa data. The short wavelength leading predominantly flexural wave is followed by trailing transients propagating away from the load.

(cf. Squire *et al.* 1996). If $|\eta| < h$ is adopted as a suitable criterion for the validity of the linearity assumption, we note that it is satisfied for the deflections shown in figures 2–6, but of course not when the deflection predicted for the steadily moving load is singular – most notably at the critical load speed $V = c_{min}$, which prompted the inclusion of anelasticity and nonlinearity in the modelling (cf. Squire *et al.* 1996; Parau & Dias 2002).
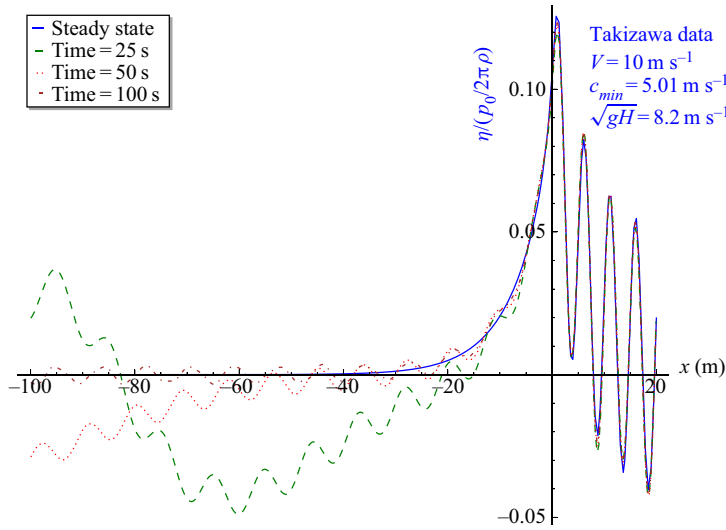
Figure 6. The deflection for the impulsively started supercritical load speed $V = 10\,\mathrm{m\,s^{-1}} > \sqrt{gH}$ at 25, 50 and 100 s for the Takizawa data. The transients behind the load propagate away rather slowly as the shadow zone develops.

4. Response due to a uniformly accelerating line load

In the next two sections we consider the response due to a uniformly accelerating load following Miles & Sneyd (2003). In this section, we consider a constant acceleration from time $t = 0$ such that $X(t) = \frac{1}{2}At^2$ $(t > 0)$, while in the next section we consider constant deceleration, $(-A)$, from the initial constant speed V such that $X(t) = Vt - \frac{1}{2}At^2$, $t > 0$. Since in §5 we also compare the deflection produced by a load decelerating at a constant rate $A = -1\,\mathrm{m\,s^{-2}}$ with the deflection produced by a load initially decelerating at the constant rate $A = -1\,\mathrm{m\,s^{-2}}$, then decelerating at the increased constant rate $A = -4\,\mathrm{m\,s^{-2}}$ until it comes to rest and then at rest, we find it convenient to derive the general expression obtained by breaking the interval $[0, t]$ into sub-intervals $0 = T_0 < T_1 < T_2 \cdots < T_J < t$ and summing the contributions from each sub-interval such that

$$
\begin{aligned}
-\frac{\tanh kH}{c} &\int_0^t \exp(-ikX(\tau))\sin kc(t - \tau)\,\mathrm{d}\tau \\
&= -\frac{\tanh kH}{c} \sum_{n=0}^{J-1} \int_{T_n}^{T_{n+1}} \exp(-ikX(\tau))\sin kc(t - \tau)\,\mathrm{d}\tau \\
&\quad -\frac{\tanh kH}{c} \int_{T_J}^t \exp(-ikX(\tau))\sin kc(t - \tau)\,\mathrm{d}\tau.
\end{aligned}
\tag{4.1}
$$

Thus when A_n denotes the constant acceleration or deceleration of the load in the interval $T_n \le t \le T_{n+1}$ and V_n denotes the speed at $t = T_n,$, we have that

$$
-\int_{T_n}^{T_{n+1}} \exp(-ikX(\tau))\sin kc(t - \tau)\mathrm{d}\tau
\tag{4.2}
$$

is equal to

$$\frac{\exp(-\mathrm{i}k\,[X(T_n) + V_n(t - T_n)])}{2k}\left[\frac{\exp(\mathrm{i}k(c + V_n)(T_{n+1} - T_n)) - 1}{c + V_n}\right.$$
$$\left. + \frac{\exp(-\mathrm{i}k(c - V_n)(T_{n+1} - T_n)) - 1}{c - V_n}\right] \tag{4.3}$$

for a load moving at a constant speed and

$$\mathrm{i}\frac{\exp(-\mathrm{i}kX(T_n))}{2}\left[\exp(\mathrm{i}kc(t - T_n))I_n(T_{n+1} - T_n, c)\right.$$
$$\left. - \exp(-\mathrm{i}kc(t - T_n))I_n(T_{n+1} - T_n, -c)\right] \tag{4.4}$$

for an accelerating load where $\gamma_n^2 = kA_n/2$, $\alpha_n = (c + V_n)/A_n$,

$$I_n(t, c) = \frac{\exp(\mathrm{i}\gamma_n^2\alpha_n^2)}{\gamma_n}[\mathcal{F}^*(\gamma_n(t + \alpha_n) - \mathcal{F}^*(\gamma_n\alpha_n)], \tag{4.5}$$

and

$$\mathcal{F}(z) = \int_0^z \mathrm{e}^{\mathrm{i}s^2}\,\mathrm{d}s = \sqrt{\frac{\pi}{2}}C\left(\sqrt{\frac{2}{\pi}}z\right) + \mathrm{i}\sqrt{\frac{\pi}{2}}S\left(\sqrt{\frac{2}{\pi}}z\right) \tag{4.6}$$

is the Fresnel integral.

The solution of (2.8) may then be expressed in terms of $I_n(t, c)$. Thus taking $J = 0$, $T_0 = 0$, $V_0 = 0$, $A_0 = A$, $\gamma_0^2 = kA/2$ and $\alpha_0 = c/A$, the leftward and rightward propagating terms in (2.8) are

$$I(c)\exp(\mathrm{i}k(x + ct)) = I_0(t, c)\exp(\mathrm{i}k(x + ct)), \tag{4.7a}$$

and

$$I(-c)\exp(\mathrm{i}k(x - ct)) = I_0(t, -c)\exp(\mathrm{i}k(x - ct)), \tag{4.7b}$$

respectively.

Figures 7–9 depict deflection snapshots we found for an impulsively started uniformly accelerating load using the Takizawa data in each of the three regimes $V > \sqrt{gH}$, $c_{min} < V < \sqrt{gH}$ and $V < c_{min}$, illustrating successive contributions as anticipated for a time-dependent load speed at the end of § 1. Thus the early quasi-static form in figure 7 is supplemented by supercritical contributions when the load accelerates beyond the critical speed c_{min} (cf. figure 8) and then the gravity wave speed $\sqrt{gH}$ (cf. figure 9). The position of the load as seen by a stationary observer is here and henceforth denoted by a red or blue arrow, showing that the maximum amplitude of the deflection tends to fall further behind the load as the load speed increases. The very high constant acceleration $A = 14\,\mathrm{m\,s^{-2}}$ assumed in figures 7–9 was chosen to reconsider the calculation in Miles & Sneyd (2003). A more likely practical value $A = 1\,\mathrm{m\,s^{-2}}$ was chosen to re-calculate the response at the load speed $V = 9.8\,\mathrm{m\,s^{-1}}$ as shown in figure 10, but now with the relevant initial static response included (blue plot) for comparison with the response due to the impulsively started load (red plot). This confirms that the response is largely determined by the acceleration, with similar larger dominant deflection amplitudes and somewhat different transients behind the load. The validity of the linearity criterion $|\eta| < h$ has become less clear, however, with nonlinear theory expected to be required at later times or for heavier loads than in Takizawa's experiments (cf. Squire *et al.* 1996). We also found there is no singularity in the deflection due to the uniformly accelerating load, but could not reproduce figure 1(*c*) of Miles & Sneyd (2003).
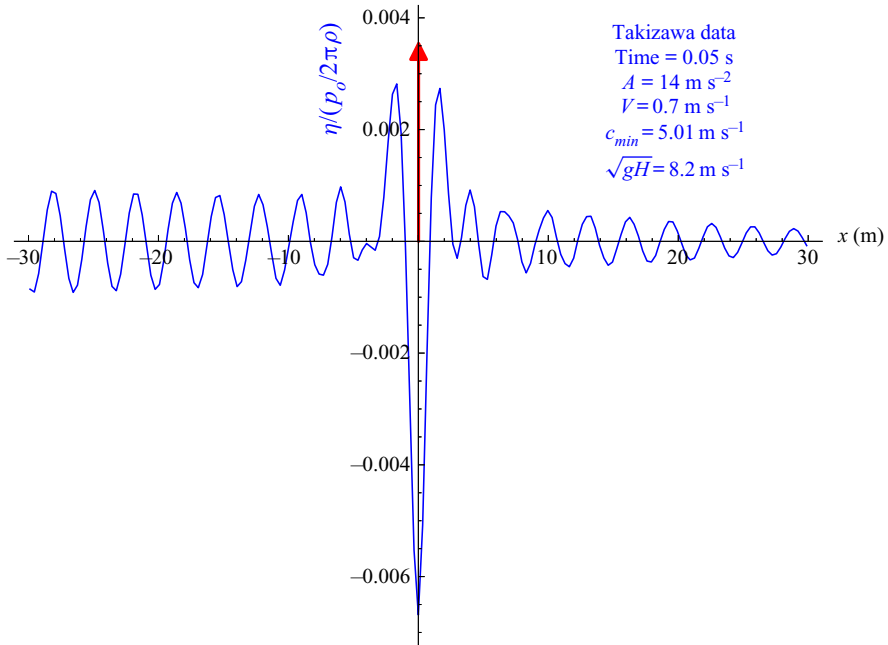
Figure 7. Subcritical response at $V = 0.7\,\text{m s}^{-1} < c_{min}$ for the impulsively started load uniformly accelerating from $t = 0$ using the Takizawa data, with a small central quasi-static feature amid leading and trailing transients.
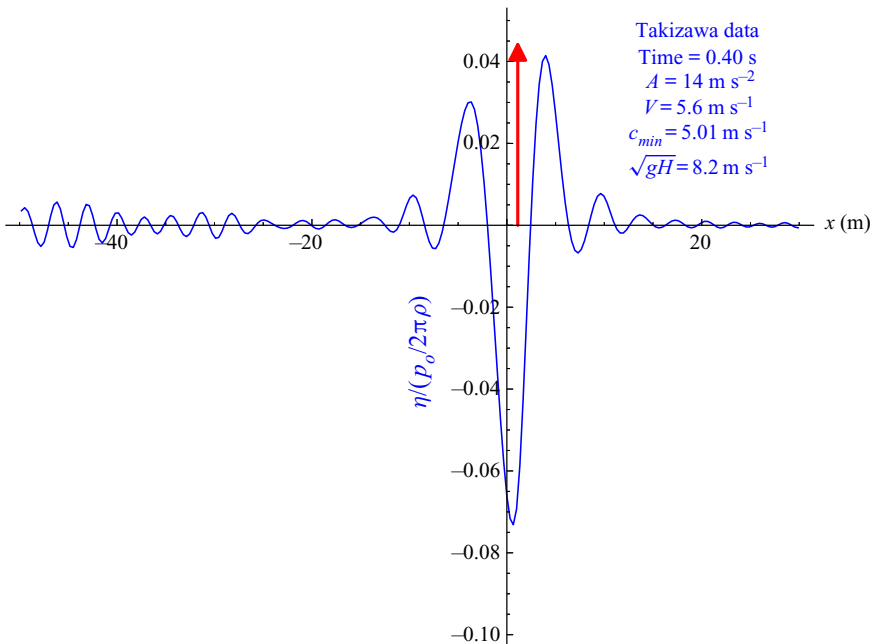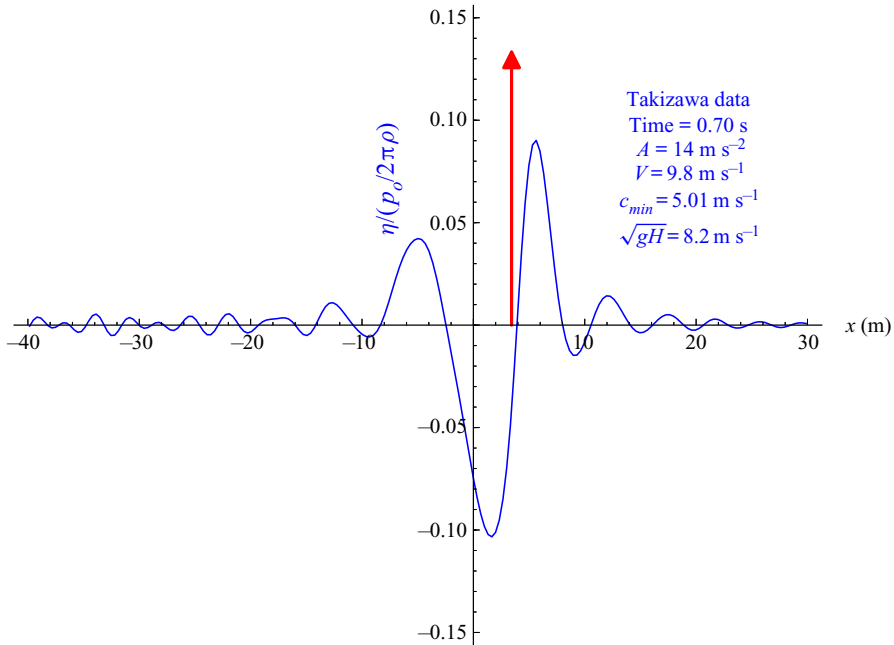

Figure 8. The supercritical response when $c_{min} < V = 5.6\,\text{m s}^{-1} < \sqrt{gH}$ for the impulsively started load uniformly accelerating from $t = 0$ using the Takizawa data, with large emerging amplitudes in the neighbourhood of the load amid persistent transients.

Figure 9. Supercritical response when $V = 9.8 \, \mathrm{m\,s^{-1}} > \sqrt{gH}$ for the impulsively started load uniformly accelerating from $t = 0$ using the Takizawa data, showing an advancing load with further enhanced leading and trailing deflections. There are even larger leading wave amplitudes, and more enlarged amplitudes trailing the load where it appears the transients persist.

5. Response due to a uniformly decelerating line load

We now proceed to determine the deflection produced by the load deceleration $(-A)$ from the initial constant speed V such that $X(t) = Vt - \frac{1}{2}At^2$, $t > 0$. In this case, taking $J = 0$, $T_0 = 0$, $V_0 = V$, $A_0 = -A$, $\gamma_0^2 = kA_0/2$ and $\alpha_0 = (V + c)/A_0$, the leftward and rightward propagating terms in (2.8) are

$$I(c) \exp(\mathrm{i}k(x + ct)) = I_0(t, c) \exp(\mathrm{i}k(x + ct)), \tag{5.1a}$$

and

$$I(-c) \exp(\mathrm{i}k(x - ct)) = I_0(t, -c) \exp(\mathrm{i}k(x - ct)), \tag{5.1b}$$

respectively.

We first reconsidered the subcritical regime, and in particular the case of a load initially moving steadily at $0.4 \, c_{min}$ that is subjected to a constant deceleration to rest in 37.75 s using the Takizawa data. As the snapshot at any arbitrary intervening time such as in figure 11 shows, the initial quasi-static form essentially moves with the load (its position again denoted by the red arrow), as the transient contributions from the deceleration and initial condition propagate away. This appears to be consistent with the response illustrated in figure 1(d) of Miles & Sneyd (2003). We again show the impulsively started case for comparison, together with the evolution of the initial condition for completeness – cf. the first term of the Fourier transform (A 2) for the deflection in Appendix A.

For the slightly different Lake Saroma data in table 1 of Dinvay *et al.* (2019), we found evolving surface and strain profiles for a 235 kg load decelerating from the steady state at the initial constant speed $V = 10 \, \mathrm{m\,s^{-1}}$ to rest, as shown in figure 12, which resembles their figure 11(b,d,f), except that the predicted deflection and strain are larger as one
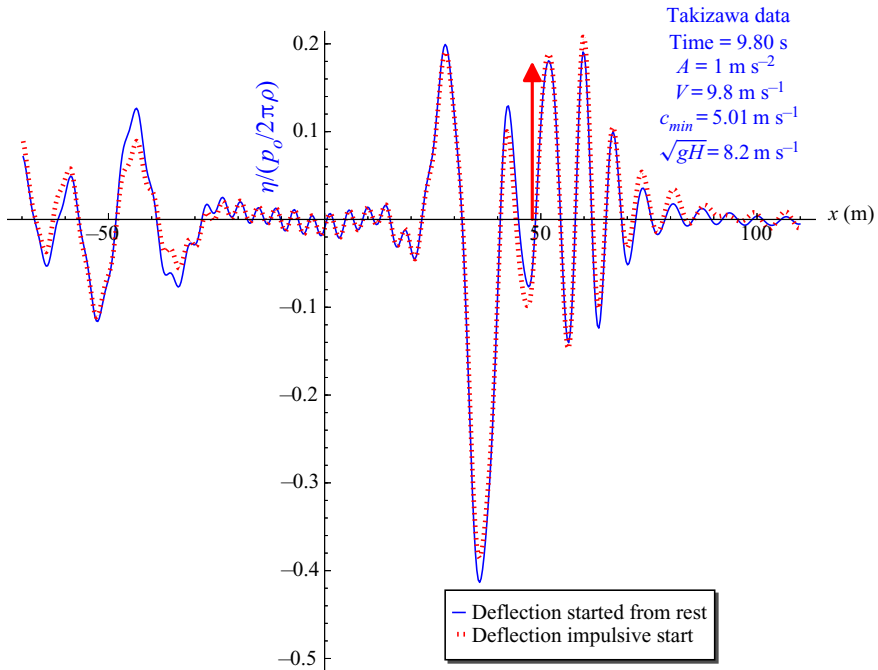
Figure 10. The supercritical response when $V = 9.8\,\mathrm{m\,s^{-1}} > \sqrt{gH}$ for the uniformly accelerating load using the Takizawa data, when the initial static response at rest is included (blue plot) and impulsively started (red plot) for confirmation that the response is determined by the acceleration. The advancing load is associated with further enlarged leading and trailing deflections, and even more persistent transients.
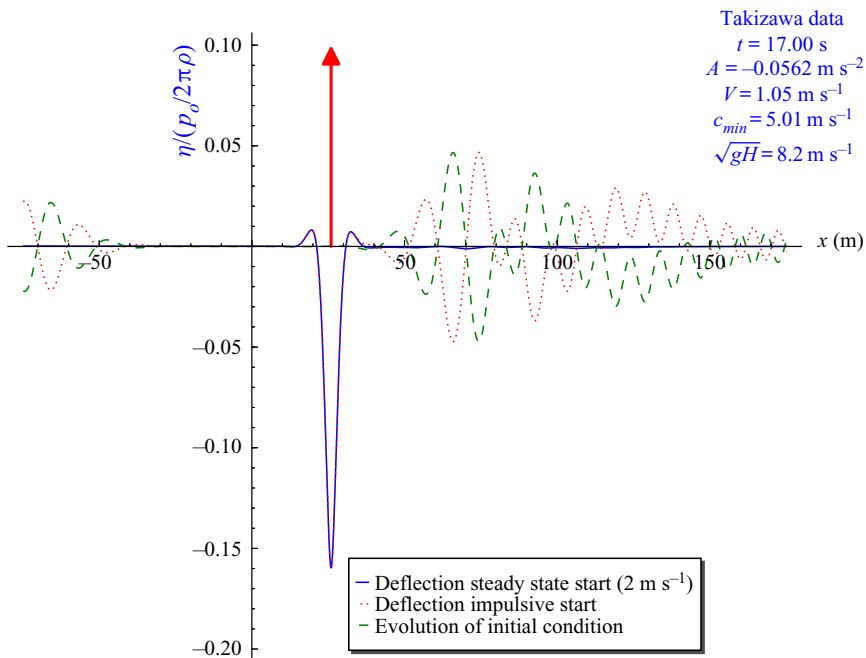

Figure 11. Snapshot at an arbitrary intervening time for a subcritical decelerating load using the Takizawa data, showing the initial quasi-static form moving with the load as the transient contributions from the deceleration and initial condition propagate away.
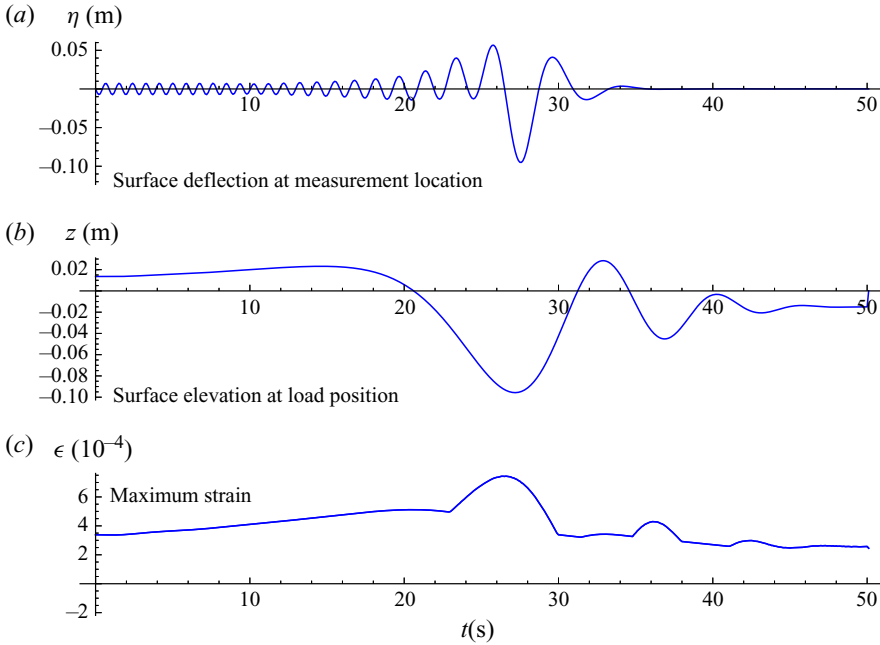
938 A2-12

Figure 12. Evolving surface and strain profiles for a 235 kg load decelerating from the steady state at the initial constant speed $V = 10\,\mathrm{m\,s}^{-1}$ to rest, using the Takizawa data in Dinvay *et al.* (2019) for direct comparison with their figure 11. The measurement location is at 200 m, and the load comes to rest after 50 s.

would expect in the simple line load model without dissipation. The strain was calculated to be $\epsilon = (h/2)\,\partial^2\eta/\partial x^2$ as in Dinvay *et al.* (2019), and in passing we observe that the linearity criterion $|\eta| < h$ is challenged but still satisfied. We then chose to further pursue the response for loads decelerating from supercritical speeds, in cases where constructive interference due to the catch up of predominantly gravity waves can reinforce the response. In particular, the results obtained for Hercules aircraft landing at McMurdo Sound and the Lockheed Electra aircraft accident in the Canadian Arctic are now discussed.

On assuming an initial supercritical load speed in landing within the wavenumber interval (k_1, k_2) identified in figure 1, we have: (i) γ ranging from $\sqrt{\frac{1}{2}k_1 A}$ to $\sqrt{\frac{1}{2}k_2 A}$ and (ii) $(V - c)/A$ ranging from zero to a maximum $(V - c_{min})/A$ and back to zero. The recommended runway length for the Hercules aircraft is approximately 1500 m, so an average deceleration A would be at least $1\,\mathrm{m\,s}^{-2}$ over a landing time of approximately a minute for a steady landing approach speed V of 120 knots or so (approximately $60\,\mathrm{m\,s}^{-1}$) as is typically recommended to pilots. This approach speed is just above the long wavelength gravity wave speed $\sqrt{gH} \simeq 58.6\,\mathrm{m\,s}^{-1}$ (in the limit $k \to 0$) shown in figure 1, when there are no trailing predominantly gravity waves supplementing the shorter wavelength leading waves before the load decelerates below $\sqrt{gH}$, until entering the subcritical regime below the critical load speed $c_{min} \simeq 22.5\,\mathrm{m\,s}^{-1}$ at wavenumber $k_{min} \simeq 2 \times 10^{-2}\,\mathrm{m}^{-1}$ where the response contribution becomes quasi-static. We adopted the parameters of Davys *et al.* in Squire *et al.* (1996), where the Young's modulus $E = 5 \times 10^9\,\mathrm{Pa}$ and the sea ice thickness $h = 2.5\,\mathrm{m}$. As previously indicated, for a time-dependent load speed the representative horizontal line in figure 1 may be envisaged to sweep down through each of the three regimes $V > \sqrt{gH}$, $c_{min} < V < \sqrt{gH}$ and $V < c_{min}$.
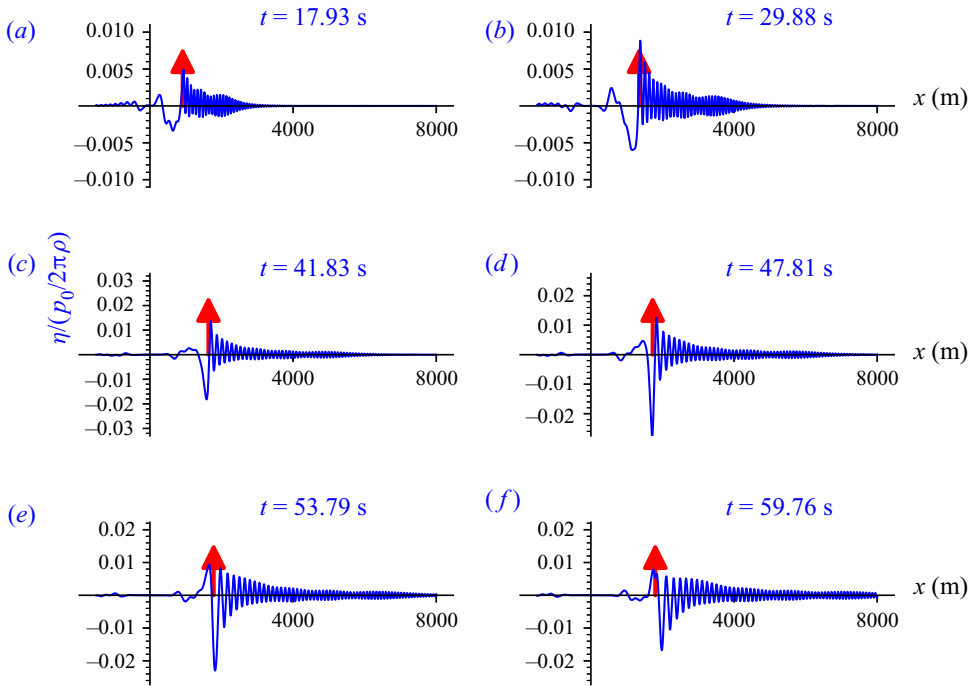
Figure 13. Deflection evolution for an impulsively started load subject to constant load deceleration $1\,\mathrm{m\,s^{-2}}$ to rest from a hypothetical initial speed of $60\,\mathrm{m\,s^{-1}}$, in the McMurdo Sound context. The successive snapshot times shown here are $t = 17.93, 29.88, 41, 83, 47.81, 53.79, 59.76$ s. The leading predominantly flexural wave stays ahead of the load, but the trailing predominantly gravity wave appears to catch up and reinforce the deflection near the load location denoted by the red arrow.

Let us first ignore the steady-state deflection from a constant supercritical approach speed $V = 60\,\mathrm{m\,s^{-1}}$, and consider a constant deceleration $A = -1\,\mathrm{m\,s^{-2}}$ until the load comes to rest after $t = 60$ s – i.e. from $V = 60\,\mathrm{m\,s^{-1}}$ just above the gravity wave speed $\sqrt{gH} \simeq 58.6\,\mathrm{m\,s^{-1}}$ for the assumed water depth $H = 350$ m, encompassing all three response regimes during the deceleration. Then, as shown in figure 13 for the McMurdo Sound parameters, we find that the early predominantly flexural contribution generated ahead of the decelerating load persists but its amplitude is soon exceeded near the load, attributed to the predominantly gravity waves generated behind continually catching up. It is also notable that there is no singularity in the predicted evolving deflection for the uniformly decelerating load.

Let us now introduce the initial steady-state deflection in the underlying ice runway calculated at the lower constant aircraft speed $V = 50\,\mathrm{m\,s^{-1}} < \sqrt{gH}$ previously considered in Davys *et al.* in Squire *et al.* (1996), as shown in figure 14. This slower aircraft speed is just above the recognised safety minimum for touchdown. A representative response during a continual constant deceleration $A = -1\,\mathrm{m\,s^{-2}}$ is shown in figure 15, where a substantial reinforcement is apparent. Thus, although the early deceleration effect over the load speed interval $\sqrt{gH} < V < 50\,\mathrm{m\,s^{-1}}$ is avoided, the subsequent response in figure 15 not only reflects the initial supercritical speed steady-state deflection in figure 14 but also a large response at the load, attributed to catchup of the trailing predominantly gravity wave produced by the deceleration effect over the range $50\,\mathrm{m\,s^{-1}} < V < c_{min}$.

The trailing predominantly gravity wave is avoided in the initial steady state at the recommended higher approach speed of approximately $60\,\mathrm{m\,s^{-1}}$ above $>\sqrt{gH}$.

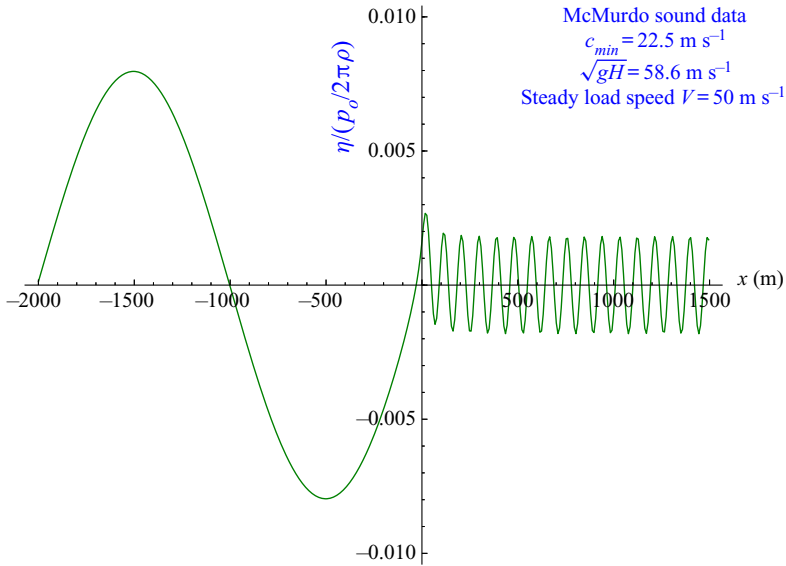Figure 14. Steady-state deflection in the McMurdo Sound ice cover of thickness 2.5 m for the constant supercritical approach speed $50 \, \mathrm{m \, s^{-1}}$ assumed in Davys *et al.* in Squire *et al.* (1996).
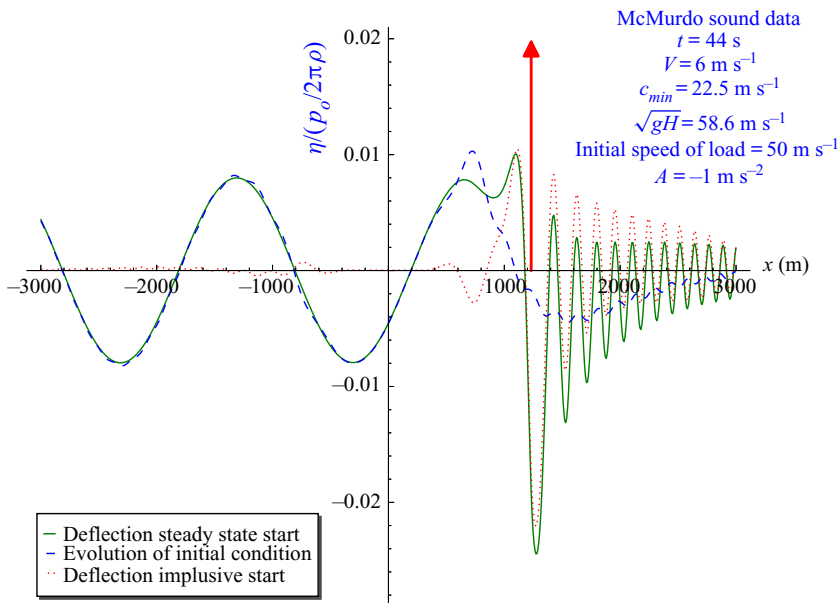

Figure 15. Localised reinforced response at the load denoted by the red arrow, attributed to catchup of the trailing predominantly gravity waves during constant deceleration $A = -1 \, \mathrm{m \, s^{-2}}$ to the load speed $V = 6 \, \mathrm{m \, s^{-1}}$ from the constant Hercules approach speed $V = 50 \, \mathrm{m \, s^{-1}}$ at McMurdo Sound previously considered by Davys *et al.* in Squire *et al.* (1996). Both the steady-state and impulsive starts are shown for comparison, together with the evolution of the initial condition.

Moreover, a pilot may apply reverse thrust retardation between 80 and 60 knots (between 40 and $30 \, \text{m s}^{-1}$ say) that can quite quickly lead to subcritical load speeds $V < c_{min}$, largely avoiding much of the predominantly gravity wave generation over the load speed range $40 \, \text{m s}^{-1} < V < c_{min} = 22.5 \, \text{m s}^{-1}$ that would otherwise accrue in the absence of the reverse thrust. For illustration, the response for the case when the load is decelerated at $A = -1 \, \text{m s}^{-2}$ from the approach speed $V = 60 \, \text{m s}^{-1}$ until $V = 40 \, \text{m s}^{-1}$ and then at $A = -4 \, \text{m s}^{-2}$ to subcritical speed in less than 5 s is compared in figure 16 with the case of constant deceleration at $A = -1 \, \text{m s}^{-2}$. Thus, whereas panel (*a*) and to some extent (*b*) in figure 13 may represent the deflection due to the common earlier deceleration at $A = -1 \, \text{m s}^{-2}$ from the landing speed of $V = 60 \, \text{m s}^{-1}$ to $V = 40 \, \text{m s}^{-1}$ in each case, the reinforcement at later times suggested by the other 4 panels in figure 13 may largely be avoided when the reverse thrust is activated. Figure 16(*c–f*) shows the deflection for the reverse thrust case (load position denoted by the blue arrow) increasingly resembles the subcritical quasi-static form whereas the constant deceleration case (load position denoted by the red arrow) also reflects the longer supercritical exposure involved, and the magnitudes are notably less than the reinforced deflection for the case of constant deceleration from the lower approach speed $V = 50 \, \text{m s}^{-1}$ shown in figure 15. Bearing in mind the known weight and dimensions of the Hercules aircraft, on introducing the $p_0/(2\pi\rho)$ factor it appears that the deflection on the thick ice at McMurdo Sound can typically be a few centimetres over a hundred metres or more, which should be measurable but hardly dangerous. The flexural-gravity waves generated were of course originally detected several kilometres away from where the Hercules aircraft were landing by John Davys and colleagues from the University of Waikato (New Zealand), which prompted many of the theoretical advances discussed in chapter 5 of Squire *et al.* (1996).

The aircraft accident off Rea Point on Melville Island in the Canadian Arctic was drawn to our attention long ago (cf. Wadhams 1997), and recently we ascertained the actual circumstances that were eventually well documented in Stevenson (1976). In 1974 a Lockheed Electra L-188 Aircraft flight with 30 passengers and 4 crew mistakenly put down onto sea ice some miles short of the intended land runway, when the cargo and cockpit broke away from the remainder of the fuselage and continued together along the ice surface for some 900 feet (274 m). Only the co-pilot and flight engineer survived, after getting out onto the ice from the cockpit before it sank completely and they were rescued by searchers from the operating company's Rea Point base. The ground speed of the aircraft before it came down was reported to be 120 knots (cf. Stevenson 1976), which is well into the high supercritical regime $V > \sqrt{gH}$ for an assumed water depth of 100 m say. Thus if we take the initial speed to be $63 \, \text{m s}^{-1}$ and again assume constant deceleration over the reported 900 feet trajectory to rest on the ice, that corresponds to $A = 7 \, \text{m s}^{-2}$ over some 9 s.

We again adopt Young's modulus $E = 5 \times 10^9 \, \text{Pa}$, an estimated new season ice thickness $h = 0.5 \, \text{m}$ and water depth $H = 100 \, \text{m}$. The initial steady-state deflection is first shown in figure 17, with the characteristic leading predominantly flexural wave and shadow zone at the load speed $63 \, \text{m s}^{-1}$ considerably above the gravity wave speed $\sqrt{gH} = 31.3 \, \text{m s}^{-1}$ for the assumed water depth of 100 m in this context. We obtained the evolution of the ice response shown in figure 18, assuming the aircraft approach speed of $63 \, \text{m s}^{-1}$ and the constant deceleration of $7 \, \text{m s}^{-2}$ over the trajectory of the cockpit and cargo on the ice. The first panel of figure 19 corresponds to the final panel in figure 18 at the time the load (cockpit and crew) comes to rest, to more clearly illustrate the antisymmetry in the deflection over an interval of 20 m or so near the load. Assuming that the load (cockpit and crew) was at least 2000 kg, as shown in figure 19 the maximum deflection is several centimetres and the strain is of order 10^{-4}. We note that the strain maximum
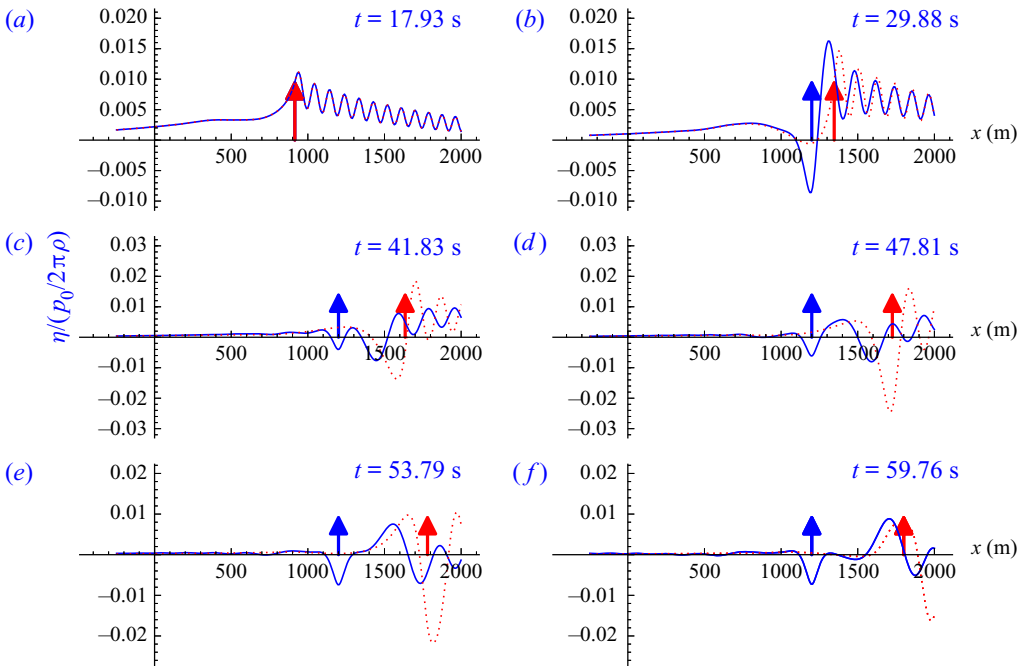
Figure 16. Response due to deceleration at $A = -1\,\mathrm{m\,s^{-2}}$ from the steady-state deflection, at the recommended higher Hercules approach speed $V = 60\,\mathrm{m\,s^{-1}}$ until the load speed $V = 40\,\mathrm{m\,s^{-1}}$, and then the increased deceleration $A = -4\,\mathrm{m\,s^{-2}}$ due to pilot activation of reverse thrust – cf. the load location denoted by the blue arrow, already distinct in panel (*b*) from the load under constant deceleration $A = -1\,\mathrm{m\,s^{-2}}$ denoted by the red arrow. The trailing predominantly gravity wave from $V = 58.6\,\mathrm{m\,s^{-1}} = \sqrt{gH}$ is evident in panel (*b*) for both cases; but in panels (*c–f*) the quasi-static form generated when $V < c_{min} = 22.5\,\mathrm{m\,s^{-1}}$ features more in the reverse thrust case than the flexural-gravity wave over the interval $c_{min} < V < \sqrt{gH}$.

coincides with the load at rest, and that it approaches the value 2.14×10^{-4} indicated in Goodman, Wadhams & Squire (1980) when the ice is most likely to fracture. Thus the constructive interference due to the predominantly gravity wave catching up may indeed account for the reported rapid sinking of the cockpit as it came to rest on the ice.

6. Conclusion

We have reconsidered the two-dimensional model for a line load moving at variable load speed on a floating ice plate, originally published in Miles & Sneyd (2003). Firstly, our calculations clarify and extend their results for an impulsively started steadily moving load using the Takizawa data, showing more completely how the responses due to a steadily moving line load on a floating ice sheet evolve in all three regimes $V > \sqrt{gH}$, $c_{min} < V < \sqrt{gH}$ and $V < c_{min}$ (cf. Squire *et al.* 1996). The deflection due to a uniformly accelerating line load was also found to always be regular and to continually increase, with maximum amplitude becoming quite large a little further behind the load as it moves through the critical speed ($V = c_{min}$) and beyond. We first calculated the contribution from the acceleration alone, but then introduced the initial quasi-static state to produce the appropriate combined result.

The response due to a uniformly decelerating load was extensively investigated, with the relevant initial steady state included or not (designated as 'impulsively started'). The singularities in the deflection predicted in the non-dissipative linear theory for a steadily
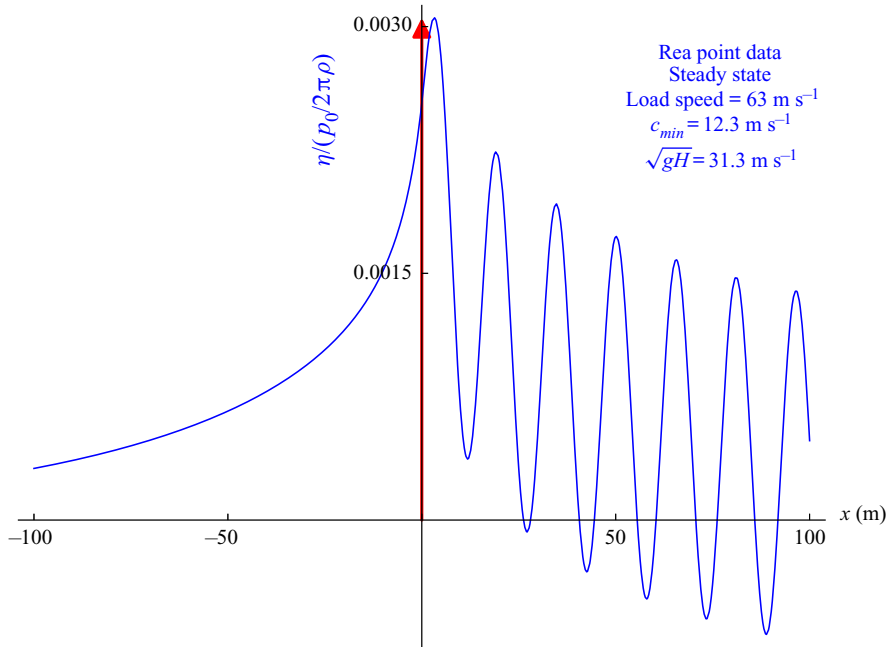
Figure 17. Steady-state deflection at the reported initial ground speed 63 m s^{-1} before the Rea Point crash.
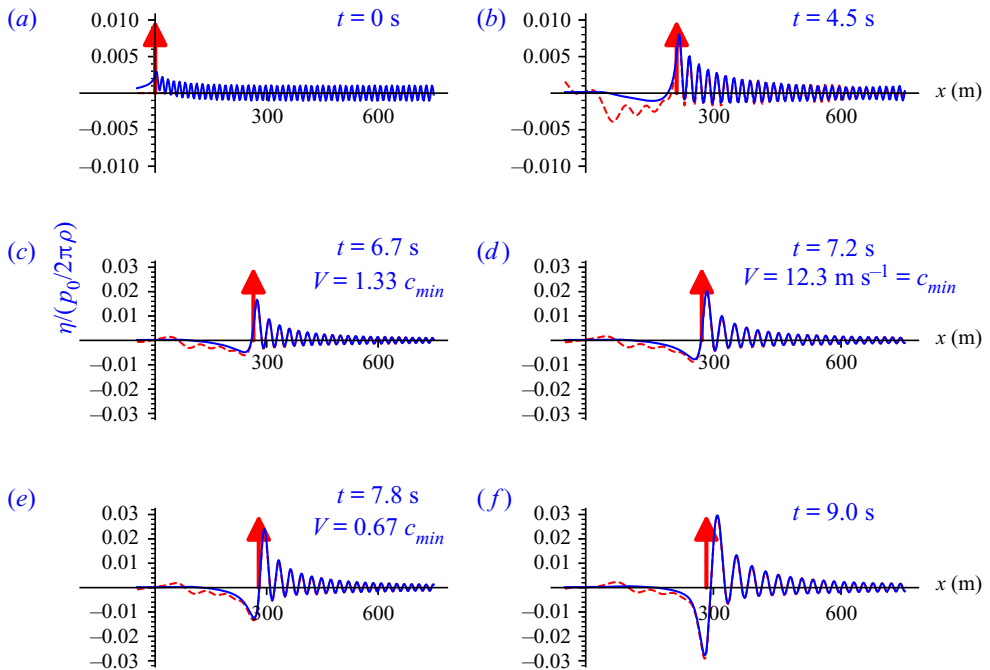

Figure 18. Deflection evolution in the Lockheed Electra crash on the sea ice off Rea Point for a constant deceleration of 7 m s^{-2} to rest at the end of the 900 feet trajectory on the ice, from the steady state at the reported aircraft approach ground speed of 63 m s^{-1} (blue curve). The red dashed curve shows the deflection has additional trailing transients when the initial steady state is ignored.
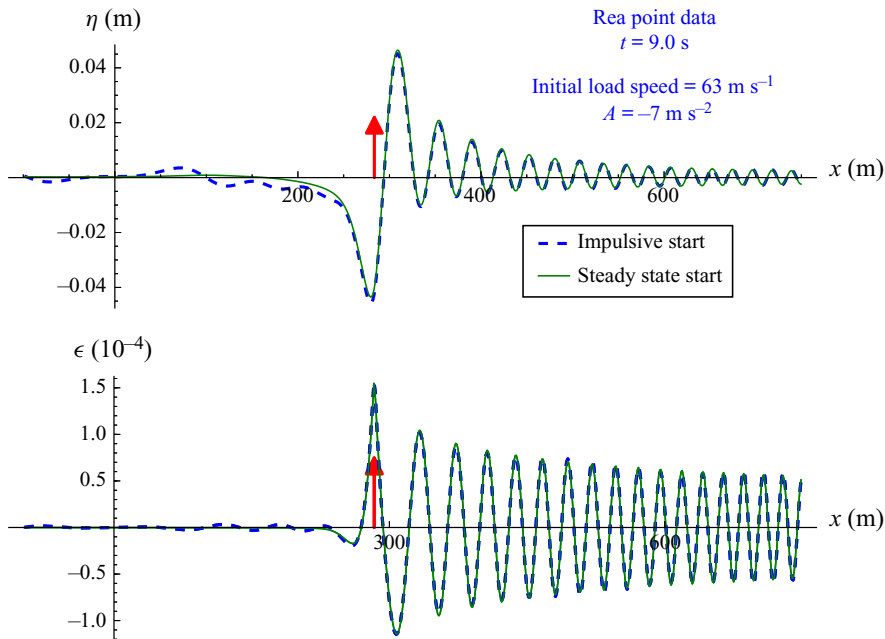
938 A2-18

Figure 19. The ice deflection in metres and associated strain in the Lockheed Electra crash off Rea Point when the initial steady-state deflection at the reported aircraft approach ground speed of $63\,\mathrm{m\,s^{-1}}$ is included, assuming a constant deceleration of $7\,\mathrm{m\,s^{-2}}$ until the load (cockpit and crew) came to rest at the end of the 900 feet trajectory on the ice. The blue dashed curve shows the deflection has additional trailing transients when the initial steady state is ignored.

moving line load (cf. Squire *et al.* 1996) were always found to be avoided when the load is uniformly decelerated, extending the conclusion in Miles & Sneyd (2003) for the uniformly accelerated load that we confirmed as mentioned above. We retained the earlier Takizawa data in showing that an initial quasi-static deflection due to a constant subcritical load speed propagates with the load as it decelerates. Evolving surface and strain profiles were also found to resemble those in figure 11 of Dinvay *et al.* (2019) for their Takizawa data, although the deflection and strain predicted by the present line load model are larger in the absence of dissipation.

We further explored the recent prediction that the deflection due to an initially supercritical load decelerating towards rest is significantly reinforced in the neighbourhood of the load, attributed to constructive interference as the erstwhile trailing predominantly gravity wave catches up with the load (cf. Dinvay *et al.* 2019). This phenomenon was investigated in the context of the landing of Hercules transport aircraft on thick sea ice at McMurdo Sound in Antarctica, and then an aircraft accident in the Canadian Arctic. The maximum deflection of several centimetres over 100 m or more may even be smaller under the recommended Hercules landing procedure when reverse thrust is applied – whereas in the accident off Rea Point in the Canadian Arctic, a deflection of several centimetres over 20 m or so on the seasonal thinner sea ice can account for the reported rapid sinking of the cockpit when it came to rest.

Linear theory originally identified the critical speed as a singularity in the deflection due to a steadily moving load on a floating ice plate, and the singularities predicted were also first investigated asymptotically for an impulsively started steadily moving load on a thin elastic or anelastic plate (cf. Squire *et al.* 1996; Nugroho *et al.* 1999; Wang *et al.* 2004).

The linearity assumption is expected to be acceptable when the maximum magnitudes of the steady-state or time-dependent deflections are smaller than the assumed thin plate thickness (as in this article), but that may not always be the case for an accelerating load or for a load decelerating from supercritical speed. The nonlinear problem for a steadily moving load (initially prompted by the predicted singularity at critical speed) has received increasing attention in recent years. However, the inclusion of anelasticity and extension of the existing nonlinear numerical calculations in Guyenne & Parau (2014) to accelerating or decelerating loads is now suggested for future investigation.

Supplementary material. Supplementary material is available at https://doi.org/10.1017/jfm.2022.109.

Declaration of interests. The authors report no conflict of interest.

Author ORCIDs.
Ⓐ Fausto Milinazzo https://orcid.org/0000-0002-6338-1547.

Appendix A

As noted in § 3, our results for the deflection due to an impulsively started load and to a load initially moving at a constant speed and then decelerating were obtained by approximating the inverse Fourier transform. While the integrand of (2.4) has no poles on the real k axis and the inverse transform can be applied directly, the integrand which results when the initial condition corresponding to an initial steady state has poles on the real axis when $V^2 - c^2 = 0$. Moreover, the results for accelerating and decelerating loads are expressed in terms of Fresnel integrals. The details of approximations and calculations required to handle these issues are provided below. Estimates of the accuracy of the methods are also given.

A.1. *Approximating the inverse Fourier transform*

As in Miles & Sneyd (2003), the integral with respect to t corresponding to an impulsively started load steadily moving which was previously uniformly accelerating or decelerating is evaluated analytically. The integral in k in (2.4) is approximated as a discrete Fourier transform and the fast Fourier transform algorithm is used to obtain an approximation of the deflection. The discretisation starts by selecting K_{max}, corresponding to the largest wavenumber to be resolved and the interval $-K_{max} < k < K_{max}$ is sub-divided into N equal parts of size $\Delta k = 2K_{max}/N$. The interval on which the deflection is to be approximated given by $-LH < x < LH$, where $L > 0$ and H is the depth of the water, is also sub-divided into N equal parts of size $\Delta x = 2LH/N$. The result is the familiar relationship between the discrete Fourier transform of the deflection at the points $k_j = j \, \Delta k$ for j from $-N$ to N and the approximation of the deflection at $x_j = j \, \Delta x$ for j from $-N$ to N. Provided that $\Delta x \, \Delta k = 2\pi/N$ the fast Fourier transform algorithm can be used to obtain the discrete approximation of the deflection from its Fourier transform.

For fixed N, $\Delta k = \pi/LH$ and $K_{max} = (N/2)(\pi/LH)$ so that L and N must be selected such that the contribution to the integral in (2.4) for $|k| > K_{max}$ is sufficiently small. For the results presented in this article, $N = 8192$ and $L = 100$. Values of N between 1024 and 16 384 and values of L between 100 and 200 were used to assess the accuracy of our approximations. As a strong accuracy test for the Rea Point data, we adopted the initial speed 63 m s^{-1} and the small deceleration of -1 m s^{-2} to rest at time $t = 63$ s. In figure 20 where $L = 100$ is used in all cases, the blue curve corresponds to the deflection obtained when $N = 8192$, the red circles when $N = 4096$, the green circles when $N = 16\,384$ and the black circles to numerical integration in (2.8) from 0 to $2K_{max}$. Figure 21 compares
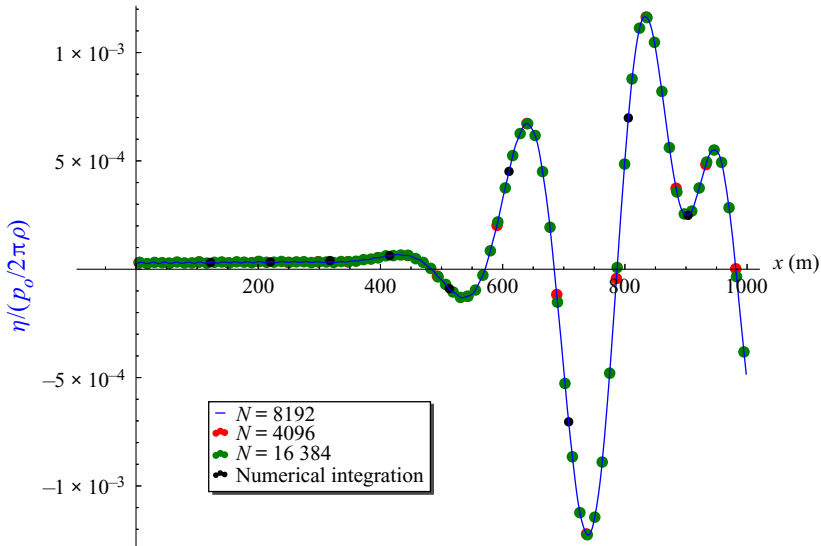
Figure 20. The computation for the Rea Point data using $N = 4096$, 8192 and $16\,384$ with $L = 100$. The blue curve corresponds to the deflection obtained when $N = 8192$ and the coloured circles denote the other N values, as indicated in the legend and stated in the text.
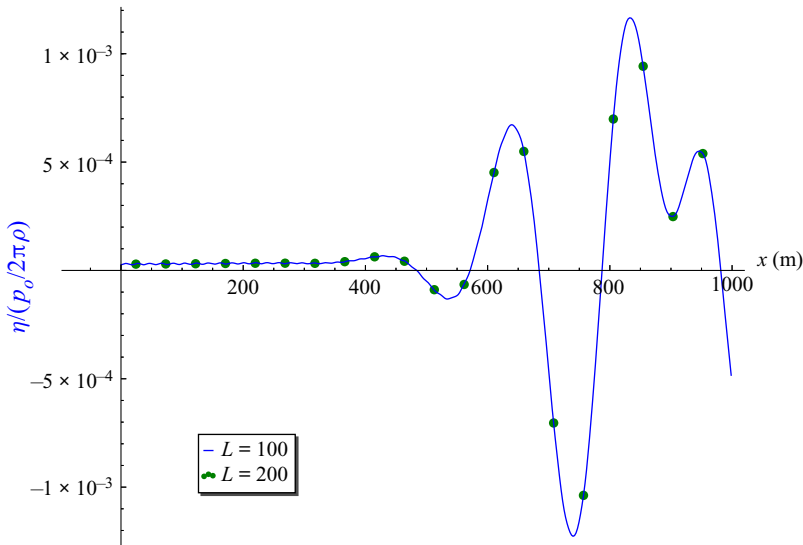

Figure 21. The computation for the Rea Point data using $L = 100$ and 200 with $N = 8192$. The blue curve corresponds to $L = 100$ and the green circles to $L = 200$, as indicated in the legend and stated in the text.

the deflections computed using $N = 8192$, where the blue curve corresponds to $L = 100$ and the green circles to $L = 200$. The accuracy is impressive, although larger values of N could be needed for larger time t than involved in our numerical calculations.

A.2. *Approximating the Fresnel integrals*

The Fresnel integrals were approximated using formulae that appear in chapter 7 of Abramowitz & Stegun (1964) using the series expansions for $|z| < 3$ and asymptotic expansions for $|z| > 3$ to evaluate the real and imaginary parts of $\mathcal{F}(z) = \int_0^z e^{is^2} \, ds$. Specifically, the first 20 terms of the series expansions 7.3.12 and 7.3.14 were used for $|z| < 3$ together with 7.3.9 and 7.3.10 and the first terms of the asymptotic expansions 7.3.27 and 7.3.28 for $|z| \geq 3$. Values obtained using these approximations were compared with values shown in the tables on pages 320–321 in the Handbook, which demonstrated an accuracy better than 10^{-4}. The accuracy in approximating $I(c)$ and $I(-c)$ was usually sufficient. However, if γt is small the differences taken in evaluating $I(c)$ and $I(-c)$ respectively could lead to inaccurate approximations, so in that case the source integrals such as $(1/\gamma) \int_{-\gamma\alpha}^{\gamma(t-\alpha)} e^{is^2} \, ds$ were approximated numerically using Romberg integration.

A.3. *The initial condition*

The results in Miles & Sneyd (2003) envisage loads started impulsively at time $t = 0$, but for loads initially moving at constant speed V the Fourier transform of the deflection becomes

$$-\frac{\tanh kH}{k} \left[\frac{\cos kct - i\frac{V}{c}\sin kct}{c^2 - V^2} + \frac{k}{c} \int_0^t \exp(-ikX(\tau)) \sin kc(t - \tau) \, d\tau \right]. \quad \text{(A1)}$$

The first term is the Fourier transform at time t of the component of the deflection due to the evolution of the initial condition and the second term is the Fourier transform of the component of the deflection at time t due to the moving load at the position $X(t)$. Since the second term has no poles on the real k axes for the class of load positions $X(t)$ considered in this article, the discrete inverse Fourier transform can be applied directly to obtain an approximation to its inverse Fourier transform. The first term has poles on the real k axes at points where $c^2 - V^2 = 0$ and consequently for $V > c_{min}$ the discrete Fourier transform cannot be applied directly. However, this term can be re-written in the form

$$-\frac{\tanh kH}{k} \left[\frac{\cos kct - i\frac{V}{c}\sin kct}{c^2 - V^2} \right] = \frac{\tanh kH}{c + V} t \left[\sin\frac{k(c + V)t}{2} \operatorname{sinc}\frac{k(c - V)t}{2} \right.$$

$$+ i\frac{V}{c} \left[\cos\frac{k(c + V)t}{2} \operatorname{sinc}\frac{k(c - V)t}{2} - \operatorname{sinc}(kVt) \right] \right]$$

$$- \frac{\tanh kH}{k} \frac{\exp(-ikVt)}{c^2 - V^2}. \quad \text{(A2)}$$

The term within the outside square brackets is regular on the real k axis so that the inverse Fourier transform of the corresponding expression can be approximated using the discrete inverse Fourier transform. The inverse Fourier transform of the last term (the steadily moving load contribution) can be evaluated analytically using the method of residues. The details of the contour integration can be found in the online Supplementary Materials available at https://doi.org/10.1017/jfm.2022.109. See also Davys *et al.* and Schulkes & Sneyd discussed in chapter 5 of Squire *et al.* (1996).

As an illustration, figure 22 shows the steady-state solutions corresponding to the load moving in the three speed regimes: $V < c_{min}$, $c_{min} < V < \sqrt{gH}$ and $V > \sqrt{gH}$.
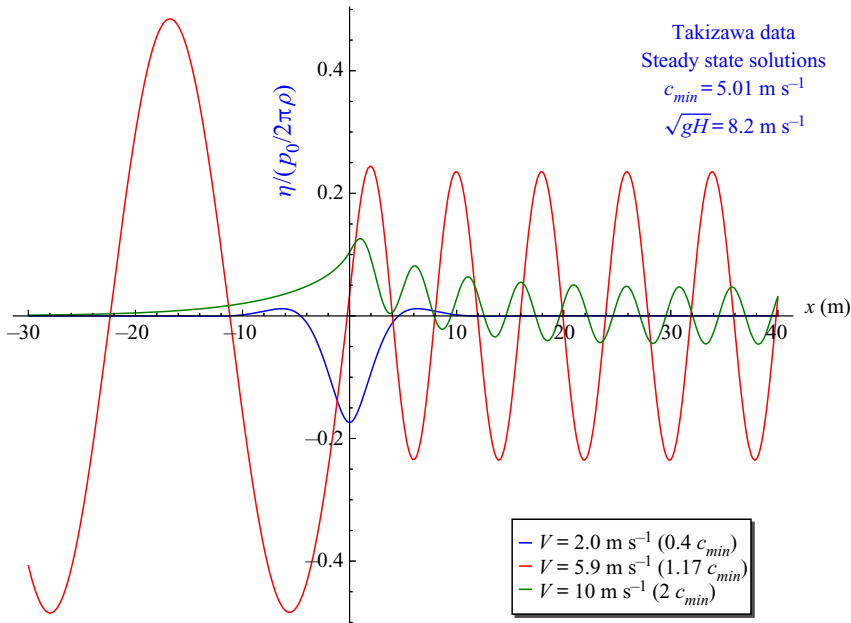
Figure 22. Steady-state deflections at the constant subcritical and supercritical speeds consistent with the three limiting results produced in § 3 for the Takizawa data.

REFERENCES

ABRAMOWITZ, M. & STEGUN, I. (Eds) 1964 *Handbook of Mathematical Functions*. Applied Mathematics Series, vol. 55. National Bureau of Standards.

BABAEI, H., VAN DER SANDEN, J., SHORT, N. & BARRETTE, P. 2016 Lake ice cover deflection induced by moving vehicles: comparing theoretical results with satellite observations. In *TAC 2016: Efficient Transportation – Managing the Demand – 2016 Conference and Exhibition of the Transportation Association of Canada.*.

BELTAOS, S. 1981 Field studies on the response of ice sheets to moving loads. *Can. J. Civ. Engng* **8**, 1–8.

DAS, S., SAHOO, T. & MEYLAN, M. 2018 Flexural-gravity wave dynamics in two-layer fluid: blocking and dead water analogue. *J. Fluid Mech.* **854**, 121–145.

DINVAY, E., KALISCH, H. & PARAU, E. 2019 Fully dispersive models for moving loads on ice sheets. *J. Fluid Mech.* **876**, 122–149.

GOODMAN, D., WADHAMS, P. & SQUIRE, V. 1980 The flexural response of a tabular ice island to ocean swell. *Ann. Glaciol.* **1**, 23–27.

GUYENNE, P. & PARAU, E. 2014 Finite-depth effects on solitary waves in a floating ice sheet. *J. Fluids Struct.* **49**, 242–262.

MATIUSHINA, A., POGORELOVA, A. & KOZIN, V.M. 2016 Effect of impact load on the ice cover during the landing of an airplane. *Intl J. Offshore Polar Engng* **26**, 6–12.

MILES, J. & SNEYD, A. 2003 The response of a floating ice sheet to an accelerating line load. *J. Fluid Mech.* **497**, 435–439.

NUGROHO, W., WANG, K., HOSKING, R. & MILINAZZO, F. 1999 Time-dependent response of a floating flexible plate to an impulsively started steadily moving load. *J. Fluid Mech.* **381**, 337–355.

PARAU, E. & DIAS, F. 2002 Nonlinear effects in the response of a floating ice plate to a moving load. *J. Fluid Mech.* **460**, 281–305.

POGORELOVA, A. 2008 Wave resistance of an air-cushion vehicle in unsteady motion over an ice sheet. *J. Appl. Mech. Tech. Phys.* **49**, 71–79.

SQUIRE, V., HOSKING, R., KERR, A. & LANGHORNE, P. 1996 *Moving Loads on Ice Plates*. Kluwer Academic Publishers. Also Arkiv, Springer (2012).

STEVENSON, W. 1976 ASN Aircraft accident Lockheed L-188PF Electra CF-PAB Rea Point Airfield, NT (YOX), Technical report, Flight Safety Foundation, Edmonton, AB. www.flightsafety.org.

VAN DER SANDEN, J. & SHORT, N. 2017 Radar satellites measure ice cover displacements induced by moving vehicles. *Cold Reg. Sci. Technol.* **133**, 56–62.

WADHAMS, P. 1997 Review of "moving loads on ice plates", Kluwer (1996). *Polar Record* **33**, 73–74.

WANG, K., HOSKING, R. & MILINAZZO, F. 2004 Time-dependent response of a floating viscoelastic plate to an impulsively started moving load. *J. Fluid Mech.* **521**, 295–317.